Angewandte Chemie

DOI: 10.1002/ange.201403817

Mesoporous Materials

Highly Ordered Mesoporous Tungsten Oxides with a Large Pore Size and Crystalline Framework for H_2S Sensing**

Yuhui Li, Wei Luo, Nan Qin, Junping Dong, Jing Wei, Wei Li, Shanshan Feng, Junchen Chen, Jiaqiang Xu, Ahmed A. Elzatahry, Mahir H. Es-Saheb, Yonghui Deng, and Dongyuan Zhao*

Abstract: *An ordered mesoporous WO_3 material with a highly crystalline framework was synthesized by using amphiphilic poly(ethylene oxide)-b-polystyrene (PEO-b-PS) diblock copolymers as a structure-directing agent through a solvent-evaporation-induced self-assembly method combined with a simple template-carbonization strategy. The obtained mesoporous WO_3 materials have a large uniform mesopore size (ca. 10.9 nm) and a high surface area (ca. 121 $m^2 g^{-1}$). The mesoporous WO_3-based H_2S gas sensor shows an excellent performance for H_2S sensing at low concentration (0.25 ppm) with fast response (2 s) and recovery (38 s). The high mesoporosity and continuous crystalline framework are responsible for the excellent performance in H_2S sensing.*

Hydrogen sulfide (H_2S), a malodorous and toxic gas, is produced or can be a byproduct of several processes, such as oil refining, coal or natural gas manufacturing, fuel cells, or food processing industries. H_2S is dangerous for human health, which can lead to personal distress at low concentration and even cause death once its concentration is higher than 250 ppm.[1] As a result, great effort has been devoted to developing nanomaterials for fabricating highly sensitive and selective H_2S sensors. Recently, mesoporous semiconductor metal oxides have attracted tremendous interest owing to their unique physical and chemical properties, and potential applications for gas sensing[2] and catalysis.[3] Gas sensing involves the adsorption–desorption and even catalytic reactions on the materials surfaces. Porous materials with high surface areas and uniform channels favor the gas diffusion and host–guest interactions. Previous reports[4] have shown that the sensitivity was largely dependent on the specific surface area and framework interconnectivity. With the same surface area, larger pores can ensure a better sensitivity. The sensitivity of the mesoporous semiconductor metal oxide-based gas sensors was superior to that of conventional sensors. Compared with nanoparticles, ordered mesoporous metal oxides with a large pore size and highly crystalline framework can offer a high surface area and better interconnectivity. At present, mesoporous metal oxides for gas-sensing applications can be synthesized through many approaches,[5–9] such as conventional sol–gel synthesis procedures,[5] chemical vapor deposition (CVD),[6] spray pyrolysis,[7] and precipitation reactions.[8] However, these methods usually lead to mesoporous metal oxides with poor crystallinity, and an ill-defined mesostructure. High crystallinity and a continuous metal oxide nanoarchitecture with a high porosity and controlled pore sizes are highly desired for maximizing gas sensing performance.[2d,10] Among various metal oxide semiconductors, tungsten oxide (WO_3) has been considered as a promising sensing material for the detection of H_2S.[4b,11] The other mesoporous metal oxides with crystalline frameworks, such as TiO_2,[12] Nb_2O_5,[3b,13] CeO_2,[14] and SnO_2,[15] have been synthesized by using non-pluronic copolymers as templates. Regarding mesoporous WO_3, most of the studies are associated with amorphous or with poorly crystalline frameworks;[11a,16] high crystallization was rarely been reported.[3f–g] The crystallinity can be improved by annealing at high temperatures; however, the ordered structure typically collapses during the process, leading to a low surface area.[3i,16a,c] High specific surface areas and crystalline frameworks are critical parameters for gas-sensing materials. Previously, we found that the amphiphilic diblock copolymer poly(ethylene oxide)-*b*-polystyrene (PEO-*b*-PS) can convert into rigid amorphous carbon during heat treatment in inert atmosphere, and the resulting

---

[*] Y. H. Li, W. Luo, J. Wei, W. Li, S. S. Feng, J. C. Chen,
Prof. Dr. Y. H. Deng, Prof. Dr. D. Y. Zhao
Department of Chemistry, Advanced Materials Laboratory, and
State Key Laboratory of Molecular Engineering of Polymers
Fudan University, Shanghai 200433 (P. R. China)
E-mail: yhdeng@fudan.edu.cn

N. Qin, Dr. J. P. Dong, Prof. Dr. J. Q. Xu
Department of Chemistry, College of Science
Shanghai University, Shanghai 200444 (P. R. China)

Dr. A. A. Elzatahry
Department of Chemistry-College of Science
King Saud University, Riyadh 11451 (Saudi Arabia)
and
Polymer Materials Research Department, Advanced Technology and New Materials Research Institute, City for Scientific Research and Technology Applications
New Borg El-Arab City, P.O. Box: 21934, Alexandria (Egypt)

Dr. M. H. Es-Saheb
Mechanical Engineering Department, King Saud University
P.D. Box 800, Riyadh 11421 (Saudi Arabia)

[**] This work was supported by the State Key 973 Program of PRC (2013CB934104 and 2012CB224805), the NSF of China (51372041 61071040 and J1103304), the specialized research fund for the doctoral program of higher education of China (20120071110007), the innovation program of Shanghai Municipal Education Commission (13ZZ004), the Shanghai Rising Star Project of STCSM (12QH1400300), and the Program for New Century Excellent Talents in University (NCET-12-0123). We extend our appreciation to the Deanship of Scientific Research at King Saud University for funding the work through the research group project No RGP-VPP-036.

Supporting information for this article is available on the WWW under http://dx.doi.org/10.1002/anie.201403817.

carbon species can prevent the collapse of mesostructured walls during high-temperature crystallization of titania and niobia.[3b,e] However, to our knowledge, ordered mesoporous WO_3 with a high crystallinity and large pore size has rarely been reported owing to the difficulty in controlling the co-assembly of block copolymers and tungsten oxide precursors and also mesostructure stability at high temperature.

Herein, we report a template-carbonization strategy to synthesize a crystalline mesoporous WO_3 with well-ordered mesopores by using high-molecular weight PEO_{117}-*b*-PS_{198} ($M_n = 25\,850\ \mathrm{g\,mol^{-1}}$) as a structure-directing agent. The synthesis is based on the carbonization of PS into amorphous carbon residual to support the ordered mesostructure during the framework crystallization. The mesoporous WO_3 obtained after removing carbon species by calcination has a large uniform mesopore size (ca. 10.9 nm), a high surface area (ca. $121\ \mathrm{m^2\,g^{-1}}$), and crystalline walls. Owing to the excellent properties of the mesostructured semiconductor, the obtained ordered mesoporous WO_3 shows excellent performance for H_2S gas sensing at low concentration (0.25 ppm) with a fast response (2 s) and recovery (38 s).

Scheme 1 illustrates the template-carbonization synthesis process. First, with the evaporation of THF from the mixed solution containing the PEO_{117}-*b*-PS_{198} molecules, HCl solution, THF, and the tungsten oxide precursor WCl_6, the PEO_{117}-*b*-PS_{198} copolymers form spherical micelles with a hydrophobic PS segment as a core surrounded by PEO segment shells. The partially hydrolyzed hydrophilic inorganic tungsten species interact with the PEO shells by hydrogen bonding. As the THF evaporation proceeds, an ordered mesostructure can be formed by a solvent-evaporation-induced self-assembly (EISA) process (Scheme 1 a). Second, the as-made inorganic–polymer hybrid is first calcined in N_2 at 350 °C. The sp^2-hybridized carbon atoms in PS blocks can be transformed into amorphous carbon, giving rise to a carbon-supported amorphous tungsten oxide mesostructure (Scheme 1 b). Finally, the product is calcined at 500 °C in air for the crystallization of the amorphous tungsten oxide walls and remove the supporting carbon species, leading to crystalline mesoporous WO_3 materials (Scheme 1 c).

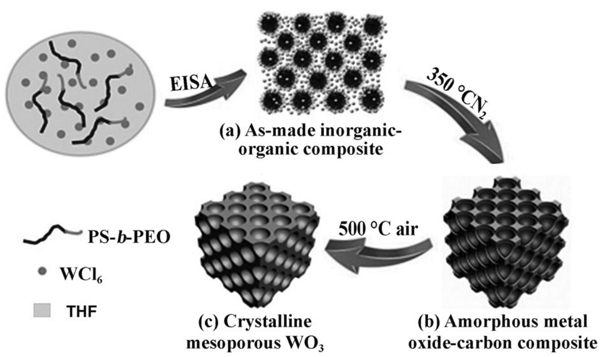

Scheme 1. The template-carbonization synthesis process of crystalline mesoporous WO_3. a) The formation of the as-made inorganic–polymer hybrid with ordered nanostructure through the solvent evaporation induced self-assembly (EISA) process; b) the formation of carbon-supported amorphous tungsten oxide by carbonization at 350 °C in N_2; c) the formation of crystalline ordered mesoporous WO_3 by subsequent heat treatment at 500 °C in air.

Small-angle X-ray scattering (SAXS) patterns (Figure 1 A) of the as-made sample and crystalline mesoporous WO_3 show four scattering peaks with q-values of 0.294, 0.566, 0.847, and 1.11 $\mathrm{nm^{-1}}$. These peaks can be indexed to the 111, 311, 500, and 533 reflections of the ordered face-centered cubic (*fcc*) mesostructure with the space group $Fm\bar{3}m$. The cell parameter of the as-made sample is calculated to be about 41.5 nm. After carbonization in N_2 at 350 °C and calcination at 500 °C in air, the first scattering peak shifts from 0.262 $\mathrm{nm^{-1}}$ to a larger q value of 0.294 $\mathrm{nm^{-1}}$, corresponding to a smaller cell parameter of 36.9 nm, owing to the framework shrinkage during the removal of the template and the crystallization of framework at high temperature. On the basis of the calculation of cell parameters, the mesostructure shrinkage is about 11.1 %.

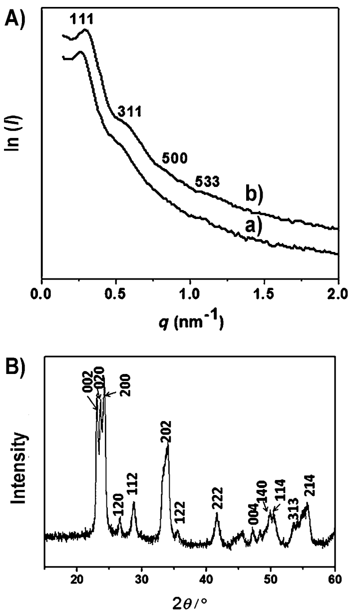

Figure 1. A) SAXS patterns of the ordered mesoporous WO_3, a) as-made and b) after calcination at 500 °C in air. B) XRD pattern of the ordered crystalline mesoporous WO_3 obtained after carbonization in N_2 at 350 °C and calcination at 500 °C in air.

The field-emission scanning electron microscope (FESEM) images taken along both the surface and cross-section of the sample clearly indicate that the obtained mesoporous WO_3 materials possess a large-domain ordered mesostructure with a uniform pore of about 10.5 nm and thick walls of about 6.6 nm (Figure 2 a,b). Transmission electron microscopy (TEM) images (Figure 2 c–e) further confirm the formation of ordered cubic mesostructure with large pores and a high degree of periodicity over large domains viewed from the [110], [100], and [211] directions of a three-dimensional (3D) cubic ($Fm\bar{3}m$) symmetry. The crystal lattice can be seen clearly from the high-resolution TEM (HRTEM; Figure 2 f), and the selected-area diffraction patterns reveal spotted diffraction rings, implying a polycrystalline feature of

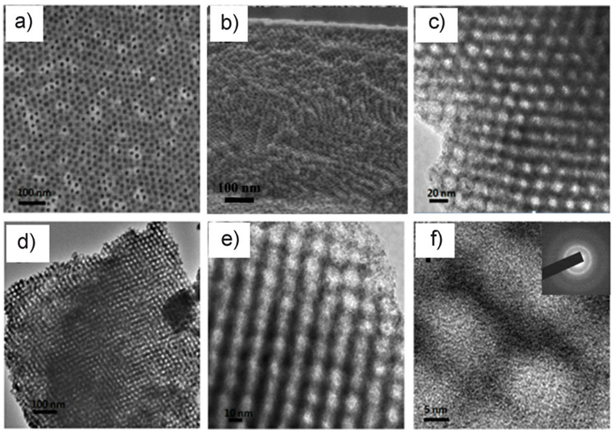

Figure 2. FESEM images: a) surface, b) cross-section; TEM images taken along the c) [110], d) [100], e) [211], and f) HRTEM image of the crystalline ordered mesoporous WO_3 obtained after carbonization in N_2 at 350 °C and calcination at 500 °C in air. The inset in (f) is the corresponding SAED pattern. Scale bars: a), b), d) 100 nm, c) 20 nm, e) 10 nm, f) 5 nm.

the pore walls (Figure 2 f, inset). Wide-angle X-ray diffraction (XRD) pattern shows well-resolved diffraction peaks in the range of 10–60° (Figure 1 B), in good agreement with the crystalline monoclinic phase of WO_3 with lattice parameters of $a = 0.7297$, $b = 0.7539$, $c = 0.7688$ nm and $\beta = 90.91°$ (JCPDS No. 43-1035). No diffraction peaks from other crystalline impurities are detected in the XRD patterns, suggesting pure crystalline WO_3. The broadening of the diffraction peaks can be ascribed to the small particle size of the WO_3 nanocrystals.

Nitrogen adsorption–desorption isotherms of the crystalline mesoporous WO_3 (Figure 3 A) show a type IV curve with a H_2-type hysteresis loop. The steep increase in the adsorption band at $P/P_0 \approx 0.8$ indicates a uniform mesopore with a large pore size. The irregular desorption curve suggests the presence of rough pore channels, which are probably due to the polycrystalline framework made of nanosized WO_3 particles. The pore size distribution derived from the adsorption branch using the BJH method shows that the pore size is uniform and centered at about 10.9 nm (Figure 3 B). The BET surface area of the ordered crystalline mesoporous WO_3 are calculated to be 121 $m^2 g^{-1}$. This value is noticeably high for mesoporous metal oxides considering the high density of tungsten oxides. The high surface area and open-pore structure of mesoporous crystalline tungsten oxide materials can provide an amplified target-receptor interface, making them an ideal candidate for many applications involving host–guest interactions, such as catalysis and gas sensing.

In this study, we explored their application for H_2S gas sensing. First, the sensor based on mesoporous WO_3 was tested towards 50 ppm H_2S gas at different temperatures ranging from 150 to 350 °C (Supporting Information, Figure S3). In this temperature range, the electrical response of the sensor increases sharply at first and then decreases rapidly with the increase of the working temperature. The measurements carried out at 250 °C show the largest response to H_2S. The electrical responses of the semiconductor oxide sensors come about from the changes in the resistances owing to the chemisorbed oxygen and target analytes.[17] The sensitivity increases with the rise of temperature owing to the increasing active energy for the chemisorptions of oxygen and H_2S species on the surface of the crystalline mesoporous WO_3. While at higher temperature, the surface coverage is reduced by a progressive gas desorption, which decreases the response of the gas sensor. This phenomenon may take the competition between the gas adsorption and desorption mechanisms into account.

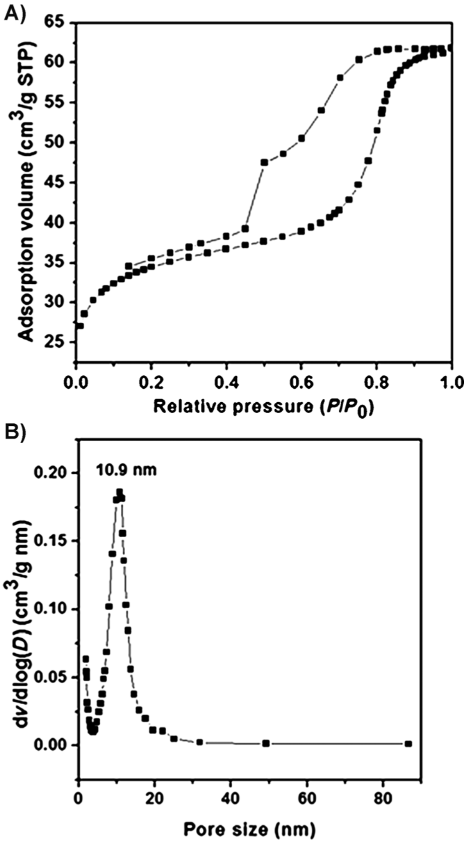

Figure 3. A) Nitrogen-sorption isotherms and B) pore-size distribution curve of the crystalline ordered mesoporous WO_3.

The dynamic electrical response of the crystalline mesoporous WO_3 to different concentration of H_2S gas (from 0.25 to 200 ppm) is shown in Figure 4 A. As the H_2S gases with different concentrations were injected into the tested chamber, the response of gas sensor rapidly increased. After vacancy (or gas off), the response can almost recover to its initial value, indicating a good reversibility of the gas sensor based on the mesoporous WO_3. The response and recovery time of the crystalline mesoporous WO_3 sensor are 2 and 38 s to 50 ppm H_2S, respectively (Figure 4 B). These results are much better than most of the H_2S gas-sensing materials reported previously, such as CuO-SnO_2 thin films,[18] ZnO nanorods,[19] tungsten oxide (nanoparticles, nanoplatelets and nanowires),[11a] Pt-loaded WO_3 thin films,[20] and CuO modified WO_3 thin films.[21] The response and recovery time were always about tens of seconds or even several minutes. Sensing layers are penetrated by oxygen and target molecules, so that

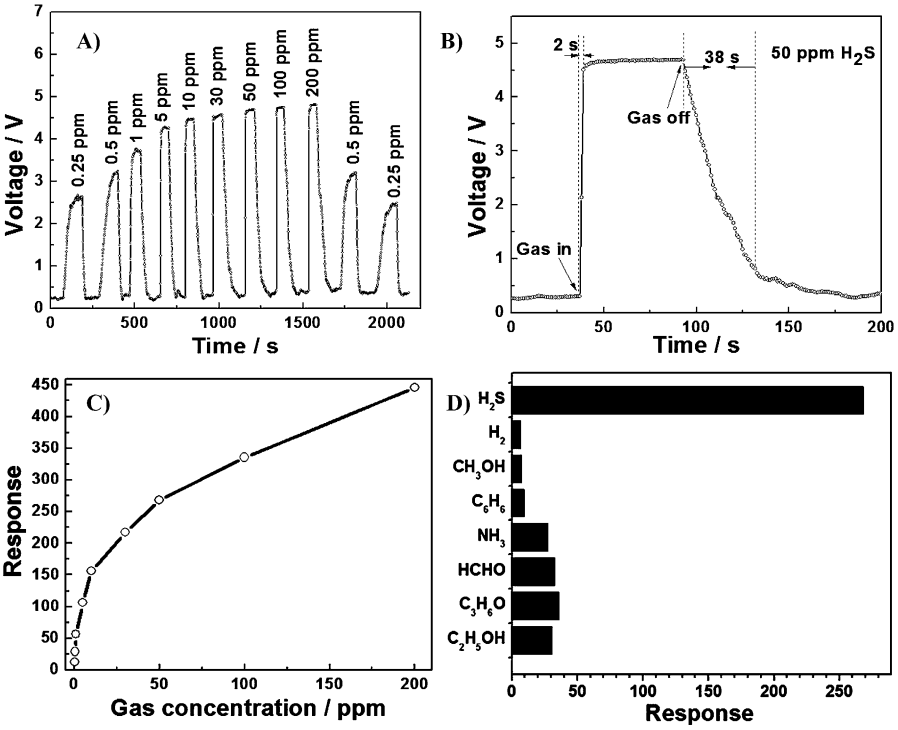

Figure 4. A) Response and recovery curve of the crystalline mesoporous WO_3 sensor to H_2S at different concentrations (0.25–200 ppm) at the working temperature of 250 °C. B) The response and recovery curve of the mesoporous WO_3-based sensor to 50 ppm of H_2S. C) The relationship between the response and the concentration of H_2S at 250 °C. D) Responses of the WO_3 sensor to different gases at 50 ppm.

a concentration gradient is formed, which depends on the equilibrium between the diffusion of the reactants and the reaction on the surface. The rate of equilibrium determines the response and recovery time. Therefore, a fast diffusion rate of gas is very important. The uniform large mesopores (ca. 10.9 nm) and high porosity of the mesoporous WO_3 sensor enhance the diffusion of gas. Simultaneously, the high crystalline framework provides fast transport of charge carriers from the surface into bulk. Therefore, it can be concluded that the open mesopore structure and crystallinity can maximize the sensitivity for gas sensing. Similar results have been reported by others.[2b,f,11d] The response of the crystalline mesoporous WO_3 sensor increases rapidly with the rise of the H_2S concentration (Figure 4C). The selectivity of a gas sensor is also an important parameter for practical application. The responses of the different types of interfering gas sources (such as H_2, CH_3OH, C_6H_6, NH_3, HCHO, acetone, and C_2H_5OH) were compared at the constant H_2S concentration of 50 ppm at 250 °C (Figure 4D). Obviously the response to H_2S is at least six times higher than those interfering gases, indicating a very impressive selectivity.

In summary, a facile template-carbonization method has been developed to synthesize the crystalline ordered mesoporous WO_3. The lab-made amphiphilic diblock copolymer PEO_{117}-*b*-PS_{198} template can provide carbon support inside pores, which can prevent the collapse of the mesostructure. So the method can make the opportunities to create other materials with defined mesoporosity and interconnectivity. The obtained ordered mesoporous WO_3 materials exhibit a large uniform mesopore size (ca. 10.9 nm), a high surface area (ca. 121 m^2g^{-1}) and crystalline frameworks. The high mesoporosity and the continuous crystalline framework are excellent properties for gas sensing. The crystalline mesoporous WO_3 were found to have a good performance for H_2S gas sensing at a low concentration (0.25 ppm) with fast response (2 s) and recovery (38 s) even in interfering gases. Based on these results, it can be expected that the obtained mesoporous WO_3 materials hold a great promise for use as gas sensor in environmental monitoring, food safety, and so on. Furthermore, the crystalline mesoporous WO_3 is expected to be used in other applications, such as the support for noble-metal catalysts, photocatalysts, and electrochemical devices.

Experimental Section

Synthesis of crystalline mesoporous WO_3: In a typical synthesis, lab-made amphiphilic diblock copolymer PEO_{117}-*b*-PS_{198} (50 mg; $M_n = 25850\ g\,mol^{-1}$, PDI = 1.09; for ^1H NMR spectra and GPC traces, see the Supporting Information, Figures S2, S3) was dissolved in THF (2.5 g), and then concentrated HCl (0.15 g, 37 wt %) was added dropwise. After stirring for 10 min, WCl_6 (0.15 g) was added in the polymer solution. Following further stirring for 2 h, the obtained dark-blue homogeneous solution was poured into petri dishes to evaporate the solvents at room temperature for 10 min, followed by solidifying the samples at 100 °C for 24 h to remove the solvents completely, leading to the formation of the inorganic–polymer hybrids. Then, the as-made products were heated and treated with a ramp of 1 °C min^{-1} to 350 °C in N_2 and held for 3 h, resulting in the carbon-supported amorphous tungsten oxide powders. The carbon was removed and crystallization of the amorphous tungsten oxide walls was carried by subsequent heat treatment with a ramp of 1 °C min^{-1} to 500 °C in air for another 2 h. The yellow-green mesoporous tungsten oxides could be obtained.

Gas sensing tests: Referring to previous work,[22] a representation of the as-fabricated gas sensor is shown in the Supporting Information, Figure S4. Gas sensing measurements were carried out on a gas sensing system of HW-30A (Hanwei Electronics Co. Ltd., P. R. China; Supporting Information, Figure S5). Before the test, the mesoporous WO_3 powder was mixed with terpineol and grounded in an agate mortar to form a paste. The resulting paste was coated on an alumina tube on which a pair of Au electrodes had been printed previously, followed by drying at 100 °C for about 2 h and subsequently annealing at 500 °C for about 2 h. Finally, a small Ni-Cr alloy coil was inserted into the tube as a heater to adjust and optimize the working temperature of the gas sensor. To improve the long-term stability, the sensors were kept at the working temperature for a week. A stationary-state gas distribution method was used for testing the gas response. The electric circuit for measuring gas response is shown in the Supporting Information, Figure S6, where a load resistor (R_L) was connected in series with a gas sensor. The circuit voltage (V_c) was set at 5 V, and the output voltage (V_{out}) was the terminal voltage of the load resistor. The working temperature of a sensor was adjusted through varying the heating voltage (V_h). The resistance of a sensor in air (R_a) or tested gas (R_g) was measured by monitoring V_{out}. Tested gases, such as H_2S, were injected into a chamber and mixed with air. The gas response of the sensor in this paper was defined as $S = R_a/R_g$ (for reducing gases) or $S = R_g/R_a$ (for oxidizing gases). The response or recovery time was expressed as the time taken for the sensor output to reach 90 % of its saturation after applying or switching off the gas in a step function. All the gas sensing measurements were carried out in air ambient with air humidity about 45 % and the chamber temperature was about 35 °C.

^{1}H NMR spectra were recorded at 25 °C on a DMX 500 MHz spectrometer (Bruker, Germany) with tetramethylsilane as an internal standard and $CDCl_3$ as a solvent. GPC was performed on an Agilent 1100 gel permeation chromatographer with refractive index detector. GPC was calibrated with monodispersed polystyrene standards. SAXS measurements were taken on a Nanostar U small-angle X-ray scattering system (Bruker, Germany) using $Cu_{K\alpha}$ radiation (40 kV, 35 mA). Nitrogen sorption isotherms were measured at 77 K with a Micromeritics Tristar 3020 analyzer. Before measurements, the samples were degassed in a vacuum at 180 °C for at least 6 h. The Brunauer–Emmett–Teller (BET) method was utilized to calculate the specific surface areas. By using the Barrett–Joyner–Halenda (BJH) model, the pore volumes and pore size distributions were derived from the adsorption branches of isotherms, and the total pore volumes (V_t) were estimated from the adsorbed amount at a relative pressure P/P_0 of 0.992. The calibration curve was obtained by using the carbon black (part no. 004-16833-00) as a reference material and nitrogen as an adsorption gas. TEM experiments were conducted on a JEOL 2011 microscope (Japan) operated at 200 kV. Field-emission scanning electron microscopy (FESEM) images were collected on the Hitachi Model S-4800 field-emission scanning electron microscope. The dried samples were directly used for the observation without any treatment.

Received: March 31, 2014

Keywords: block copolymers · gas sensing · hydrogen sulfide · mesoporous materials · tungsten oxide

---

[1] W. Cheng, E. Baudrin, B. Dunn, J. I. Zink, *J. Mater. Chem.* **2001**, *11*, 92.

[2] a) J. Zhao, T. L. Yang, Y. P. Liu, Z. Y. Wang, X. W. Li, Y. F. Sun, Y. Du, Y. C. Li, G. Y. Lu, *Sens. Actuators B* **2014**, *191*, 806; b) T. Wagner, S. Haffer, C. Weinberger, D. Klaus, M. Tiemann, *Chem. Soc. Rev.* **2013**, *42*, 4036; c) Y. X. Qin, F. Wang, W. J. Shen, M. Hu, *J. Alloys Compd.* **2012**, *540*, 21; d) S. Shao, M. Dimitrov, N. Guan, R. Koehn, *J. Mater. Chem.* **2009**, *19*, 8411; e) J. Yang, K. Hidajat, S. Kawi, *J. Mater. Chem.* **2009**, *19*, 292; f) T. Waitz, T. Wagner, T. Sauerwald, C.-D. Kohl, M. Tiemann, *Adv. Funct. Mater.* **2009**, *19*, 653; g) Y. D. Wang, I. Djerdj, M. Antonietti, B. Smarsly, *Small* **2008**, *4*, 1656; h) M. Tiemann, *Chem. Eur. J.* **2007**, *13*, 8376; i) Y. Shimizu, T. Hyodo, M. Egashira, *J. Eur. Ceram. Soc.* **2004**, *24*, 1389.

[3] a) D. Feng, W. Luo, J. Y. Zhang, M. Xu, R. Y. Zhang, H. Y. Wu, Y. Y. Lv, A. M. Asiri, S. B. Khan, M. M. Rahman, G. F. Zheng, D. Y. Zhao, *J. Mater. Chem. A* **2013**, *1*, 1591; b) J. P. Kumar, P. V. R. K. Ramacharyulu, B. Kamal, P. K. Shankar, G. K. Prasad, *Adv. Porous Mater.* **2013**, *1*, 310; c) W. Luo, Y. H. Li, J. P. Dong, J. Wei, J. Q. Xu, Y. H. Deng, D. Y. Zhao, *Angew. Chem.* **2013**, *125*, 10699; *Angew. Chem. Int. Ed.* **2013**, *52*, 10505; d) H. Tüysüz, C. Weidenthaler, F. Schüth, *Chem. Eur. J.* **2012**, *18*, 5080; e) Z. Xie, Y. G. Zhu, J. Xu, H. T. Huang, D. Chen, G. Z. Shen, *CrystEngComm* **2011**, *13*, 6393; f) J. Y. Zhang, Y. H. Deng, D. Gu, S. T. Wang, L. She, R. C. Che, Z.-S. Wang, B. Tu, S. H. Xie, D. Y. Zhao, *Adv. Energy Mater.* **2010**, *1*, 241; g) L. Li, M. Krissanasaeranee, S. W. Pattinson, M. Stefik, U. Wiesner, U. Steiner, D. Eder, *Chem. Commun.* **2010**, *46*, 7620; h) T. Brezesinski, D. Fattakhova Rohlfing, S. Sallard, M. Antonietti, B. M. Smarsly, *Small* **2006**, *2*, 1203; i) A. Taguchi, F. Schüth, *Microporous Mesoporous Mater.* **2005**, *77*, 1; j) W. Zhou, W. Li, G. F. Wang, Y. Qu, L. Wang, T. Li, G. H. Tian, K. Pan, M. X. Li, B. J. Jiang, H. G. Fu, *Adv. Porous Mater.* **2013**, *1*, 262.

[4] a) I. M. Szilágyi, S. Saukko, J. Mizsei, A. L. Tóth, J. Madarász, G. Pokol, *Solid State Sci.* **2010**, *12*, 1857; b) E. Rossinyol, A. Prim, E. Pellicer, J. Arbiol, F. Hernández-Ramírez, F. Peiró, A. Cornet, J. R. Morante, L. A. Solovyov, B. Z. Tian, T. Bo, D. Y. Zhao, *Adv. Funct. Mater.* **2007**, *17*, 1801; c) E. Rossinyol, J. Arbiol, F. Peìró, A. Cornet, J. R. Morante, B. Z. Tian, T. Bo, D. Y. Zhao, *Sens. Actuators B* **2005**, *109*, 57; d) T. Hyodo, S. Abe, Y. Shimizu, M. Egashira, *Sens. Actuators B* **2003**, *93*, 590; e) T. Hyodo, N. Nishida, Y. Shimizu, M. Egashira, *Sens. Actuators B* **2002**, *83*, 209.

[5] a) D. D. Vuong, G. Sakai, K. Shimanoe, N. Yamazoe, *Sens. Actuators B* **2005**, *105*, 437; b) D. D. Vuong, G. Sakai, K. Shimanoe, N. Yamazoe, *Sens. Actuators B* **2004**, *103*, 386; c) N. S. Baik, G. Sakai, N. Miura, N. Yamazoe, *J. Am. Ceram. Soc.* **2000**, *83*, 2983; d) N. S. Baik, G. Sakai, K. Shimanoe, N. Miura, N. Yamazoe, *Sens. Actuators B* **2000**, *65*, 97; e) N. S. Baik, G. Sakai, N. Miura, N. Yamazoe, *Sens. Actuators B* **2000**, *63*, 74.

[6] Y. Liu, E. Koep, M. Liu, *Chem. Mater.* **2005**, *17*, 3997.

[7] a) G. Korotcenkov, I. Boris, V. Brinzari, S. H. Han, B. K. Cho, *Sens. Actuators B* **2013**, *182*, 112; b) G. Korotcenkov, I. Blinov, M. Ivanov, J. R. Stetter, *Sens. Actuators B* **2007**, *120*, 679; c) G. Korotcenkov, A. Cornet, E. Rossinyol, J. Arbiol, V. Brinzari, Y. Blinov, *Thin Solid Films* **2005**, *471*, 310.

[8] N. Pinna, G. Neri, M. Antonietti, M. Niederberger, *Angew. Chem.* **2004**, *116*, 4445; *Angew. Chem. Int. Ed.* **2004**, *43*, 4345.

[9] E. R. Leite, I. T. Weber, E. Longo, J. A. Varela, *Adv. Mater.* **2000**, *12*, 965.

[10] a) T. Waitz, B. Becker, T. Wagner, T. Sauerwald, C.-D. Kohl, M. Tiemann, *Sens. Actuators B* **2010**, *150*, 788; b) T. Wagner, T. Sauerwald, C.-D. Kohl, T. Waitz, C. Weidmann, M. Tiemann, *Thin Solid Films* **2009**, *517*, 6170; c) T. Wagner, T. Waitz, J. Roggenbuck, M. Froba, C. D. Kohl, M. Tiemann, *Thin Solid Films* **2007**, *515*, 8360; d) T. Wagner, C.-D. Kohl, M. Froba, M. Tiemann, *Sensors* **2006**, *6*, 318.

[11] a) C. S. Rout, M. Hegde, C. N. R. Rao, *Sens. Actuators B* **2008**, *128*, 488; b) L. G. Teoh, Y. M. Hon, J. Shieh, W. H. Lai, M. H. Hon, *Sens. Actuators B* **2003**, *96*, 219; c) I. Jiménez, J. Arbiol, G. Dezanneau, A. Cornet, J. R. Morante, *Sens. Actuators B* **2003**, *93*, 475; d) W.-H. Tao, C.-H. Tsai, *Sens. Actuators B* **2002**, *81*, 237.

[12] a) E. Ortel, A. Fischer, L. Chuenchom, J. Polte, F. Emmerling, B. Smarsly, R. Kraehnert, *Small* **2012**, *8*, 298; b) J. Y. Zhang, Y. H. Deng, D. Gu, S. T. Wang, L. She, R. C. Che, Z. S. Wang, B. Tu, S. H. Xie, D. Y. Zhao, *Adv. Energy Mater.* **2011**, *1*, 241; c) J. Hwang, J. Kim, E. Ramasamy, W. Choi, J. Lee, *Microporous Mesoporous Mater.* **2011**, *143*, 149; d) T. Brezesinski, J. Wang, J. Polleux, B. Dunn, S. H. Tolbert, *J. Am. Chem. Soc.* **2009**, *131*, 1802; e) M. Stefik, J. Lee, U. Wiesner, *Chem. Commun.* **2009**, 2532; f) D. Fattakhova-Rohlfing, M. Wark, T. Brezesinski, B. M. Smarsly, J. Rathousky, *Adv. Funct. Mater.* **2007**, *17*, 123; g) T. Brezesinski, M. Groenewolt, A. Gibaud, N. Pinna, M. Antonietti, B. Smarsly, *Adv. Mater.* **2006**, *18*, 2260; h) D. Feng, J. Wei, M. H. Wang, Q. Yue, Y. H. Deng, A. M. Asiri, D. Y. Zhao, *Adv. Porous Mater.* **2013**, *1*, 164.

[13] a) T. Brezesinski, J. Wang, R. Senter, K. Brezesinski, B. Dunn, S. H. Tolbert, *ACS Nano* **2010**, *4*, 967; b) T. Brezesinski, C. Erpen, K. Iimura, B. Smarsly, *Chem. Mater.* **2005**, *17*, 1683; c) T. Brezesinski, M. Antonietti, M. Groenewolt, N. Pinna, B. Smarsly, *New J. Chem.* **2005**, *29*, 237.

[14] a) N. Suzuki, M. Imura, Y. Nemoto, X. Jiang, Y. Yamauchi, *CrystEngComm* **2011**, *13*, 40; b) M. Stefik, S. Mahajan, H. Sai, T. H. Epps, F. S. Bates, S. M. Gruner, O. F. J. DiSalvo, U. Wiesner, *Chem. Mater.* **2009**, *21*, 5466; c) M. C. Orilall, F. Matsumoto, Q. Zhou, H. Sai, H. D. Abruna, F. J. DiSalvo, U. Wiesner, *J. Am. Chem. Soc.* **2009**, *131*, 9389.

[15] a) Y. Wang, T. Brezesinski, M. Antonietti, B. Smarsly, *ACS Nano* **2009**, *3*, 1373; b) T. Brezesinski, A. Fischer, K. Iimura, C. Sanchez, D. Grosso, M. Antonietti, B. M. Smarsly, *Adv. Funct. Mater.* **2006**, *16*, 1433; c) J. H. Ba, J. Polleux, M. Antonietti, M. Niederberger, *Adv. Mater.* **2005**, *17*, 2509.

[16] a) L. M. Bertus, C. Faure, A. Danine, C. Labrugere, G. Campet, A. Rougier, A. Duta, *Mater. Chem. Phys.* **2013**, *140*, 49; b) P. D. Yang, D. Y. Zhao, D. I. Margolese, B. F. Chmelka, G. D. Stucky, *Nature* **1998**, *396*, 152; c) Z. J. Miao, Y. Y. Wu, X. R. Zhang, Z. M. Liu, B. X. Han, K. L. Ding, G. M. An, *J. Mater. Chem.* **2007**, *17*, 1791.

[17] a) C. X. Wang, L. W. Yin, L. Y. Zhang, D. Xiang, R. Gao, *Sensors* **2010**, *10*, 2088; b) M. E. Franke, T. J. Koplin, U. Simon, *Small* **2006**, *2*, 36.

[18] a) A. Khanna, R. Kumar, S. S. Bhatti, *Appl. Phys. Lett.* **2003**, *82*, 4388; b) R. Kumar, A. Khanna, P. Tripathi, R. V. Nandedkar, S. R. Potdar, S. M. Chaudhari, S. S. Bhatti, *J. Phys. D* **2003**, *36*, 2377.

[19] C. H. Wang, X. F. Chu, M. W. Wu, *Sens. Actuators B* **2006**, *113*, 320.

[20] Y. B. Shen, B. Q. Zhang, X. M. Cao, D. Z. Wei, J. W. Ma, L. J. Jia, S. L. Gao, B. Y. Cui, Y. C. Jin, *Sens. Actuators B* **2014**, *193*, 273.

[21] N. S. Ramgir, C. P. Goyal, P. K. Sharma, U. K. Goutam, S. Bhattacharya, N. Datta, M. Kaur, A. K. Debnath, D. K. Aswal, S. K. Gupta, *Sens. Actuators B* **2013**, *188*, 525.

[22] a) N. Qin, X. H. Wang, Q. Xiang, J. Q. Xu, *Sens. Actuators B* **2014**, *191*, 770; b) Y. Zhang, J. Q. Xu, Q. Xiang, H. Li, Q. Y. Pan, P. C. Xu, *J. Phys. Chem. C* **2009**, *113*, 3430.